RESEARCH ARTICLE

Fabrication of $Bi_{14}W_2O_{27}/Bi_2WO_6$ Photocatalyst for Improving Desulfurization of Thiophene under Simulated Sunlight Irradiation

Mohammad Ebadi[1,*], Majid Asri[1], Farshad Beshka[2]

[1] Department of Chemical Engineering, Birjand Branch, Islamic Azad University, Birjand, Iran

[2] Institute of Nanoscience and Nanotechnology, University of Kashan

ARTICLE INFO

Article History:
Received 2021-06-14
Accepted 2021-09-28
Published 2022-06-30

Keywords:
$Bi_{14}W_2O_{27}/Bi_2WO_6$, Pechini sol-gel, Nanocomposite photocatalyst, Desulfurization, Radical trapping.

ABSTRACT

In this work, novel $Bi_{14}W_2O_{27}/Bi_2WO_6$ nanocomposite was prepared by a modified Pechini sol-gel approach. The effect of the gelling agent, chelating agent and mole ratio of chelating agent to total metals was controlled to produce ultrafine $Bi_{14}W_2O_{27}/Bi_2WO_6$ nanoparticles. The as-prepared $Bi_{14}W_2O_{27}/Bi_2WO_6$ nanocomposite was characterized by XRD, FESEM, FT-IR, EDS and UV–Vis analysis. The $Bi_{14}W_2O_{27}/Bi_2WO_6$ nanostructures exhibited excellent photocatalytic desulfurization of thiophene (~90%) after 120 min of simulated sunlight irradiation. The high-efficiency of photocatalytic desulfurization of the as-prepared $Bi_{14}W_2O_{27}/Bi_2WO_6$ can be attributed to the improved visible-light absorption, ultrafine nanoparticles, and high separation and low recombination rates of charge carriers. In addition, a reliable photocatalytic desulfurization mechanism was explained using radical trapping experiment, which indicated that the photogenerated $^{\bullet}O_2^-$ and $^{\bullet}OH$ species had a significant contribution in the photocatalytic desulfurization reactions of $Bi_{14}W_2O_{27}/Bi_2WO_6$ nanocomposite. The excellent photocatalytic desulfurization efficiency, good recyclability, solar-driven, and simple synthesis of $Bi_{14}W_2O_{27}/Bi_2WO_6$ nanocomposite are promising for photocatalytic applications.

How to cite this article
Ebadi M., Asri M., Beshkar F. Fabrication of $Bi_{14}W_2O_{27}/Bi_2WO_6$ Photocatalyst for Improving Desulfurization of Thiophene under Simulated Sunlight Irradiation . J. Nanoanalysis., 2022; 9(2): 99-109. DOI: 10.22034/jna.2021.1933294.1260.

INTRODUCTION

In recent years, sulfur-containing liquid fuels release considerable values of sulfur oxide gases into the air due to combustion in transportation vehicles, which can harm human and the environment. Hence, the strict environmental legislations have been established to eliminate the sulfur oxide contaminants in the atmosphere [1-3]. For this purpose, various desulfurization technologies have been applied to produce ultra-clean liquid fuels, including hydrogenation, oxidation, adsorption, extraction, sonication, catalytic and bio-assisted desulfurization methods [3-6]. Particularly, photocatalytic oxidative desulfurization technique has attracted increasing attention because of the advantages of sun-light utilization, high-performance, moderate reaction conditions, recyclability, low-cost, safety and eco-friendly. In the photocatalytic desulfurization process, an efficient photocatalyst is the core of catalytic reaction, which can be photoexcited and generates powerful active radicals for the oxidation of sulfur compounds into non-hazardous products [7-12].

So far, various photocatalysts such as TiO_2, CeO_2, Bi_2WO_6, $CuO/BiVO_4$, $BiOI/BiPO_4$ and so on, have been employed for photocatalytic desulfurization process [1, 13, 14]. Recently, bismuth tungstate compounds owing to their layered perovskite-like structure, suitable band-gap energy (~2.7 eV), sunlight absorption, high specific surface area, non-toxicity, and physiochemical stability have been used in the various applications such as photocatalytic degradation, antibiotic removal, water splitting, oxidation reaction, full

* Corresponding Author Email: *ebadi@iaubir.ac.ir*

Table 1. The preparation conditions of the $Bi_{14}W_2O_{27}/Bi_2WO_6$ products.

Sample No.	Chelating agent	Gelling agent	Mole ratio of chelating agent to total metals
1	Tetracycline	PEG-6000	0.5:1
2	Cefixime	PEG-6000	0.5:1
3	Sulfanilamide	PEG-6000	0.5:1
4	Tetracycline	PEG-6000	1:1
5	Tetracycline	tepa	0.5:1

cell, sensor, wastewater treatment and especially photodesulfurization [13, 15-23]. However, due to the short lifetime of photogenerated electron-hole pairs in the bismuth tungstate materials, their photocatalytic activity needs to be enhanced. Up to now, various bismuth tungstate-based nanocomposites have been developed such as Nb_2O_5/Bi_2WO_6, Bi_2WO_6/TiO_2, Co_3O_4/Bi_2WO_6, Bi_2O_3/Bi_2WO_6, $MoSe_2/Bi_2WO_6$, $GO/BiOI/Bi_2WO_6$, Bi_2MoO_6/Bi_2WO_6/MWCNTs, and g-C_3N_4/Ag/Bi_2WO_6, which can reduce the recombination rate of charge carriers and subsequently improve photocatalytic performance [13, 17-19, 24, 25].

It is reported that the catalytic performance of the nanoscale materials depends on the nature, structure, purity, particle size and shape, thus it is necessary to choose an impressive approach to fabricate and control the mentioned parameters. Among the synthesis methods of nanostructures, Pechini sol–gel technique provides an easy, large-scale mass production, moderate conditions, low-cost, and eco-friendly process to optimize the homogeneity, purity and morphology of the nanomaterials. In this route, an esterification process is performed between chelating ligands and gelling agents, subsequently the as-formed polymeric network can trap precursor ions and generate homogeneous and uniform nanoparticles [26-32].

Here, we synthesized novel $Bi_{14}W_2O_{27}/Bi_2WO_6$ nanocomposite using a modified Pechini sol-gel process. It is the first time that the $Bi_{14}W_2O_{27}/Bi_2WO_6$ nanostructures were fabricated and employed for the photocatalytic desulfurization activity under simulated sunlight irradiation. The ultrafine $Bi_{14}W_2O_{27}/Bi_2WO_6$ nanostructures displayed superior photocatalytic desulfurization of thiophene (~90%) under simulated sunlight irradiation. The high photocatalytic desulfurization efficiency of the $Bi_{14}W_2O_{27}/Bi_2WO_6$ nanoparticles can be ascribed to the promoted visible-light absorption, ultrafine morphology, and high separation and low recombination rates of charge carriers. Furthermore, photodesulfurization mechanism showed that the $^{\bullet}O_2^-$ and $^{\bullet}OH$ radicals are the main species in the photocatalytic desulfurization process over $Bi_{14}W_2O_{27}/Bi_2WO_6$ product.

EXPERIMENTAL

Materials and methods

Bismuth nitrate pentahydrate ($Bi(NO_3)_3.5H_2O$), sodium tungstate (Na_2WO_4), polyethylene glycol-6000 (PEG-6000), tetraethylenepentamine (tepa), ethylenediaminetetraacetic acid disodium (EDTA-Na_2), benzoquinone (BQ), isopropanol (IPA), tetracycline, cefixime, sulfanilamide, thiophene, n-hexane, dimethylformamide (DMF), nitric acid (HNO_3) and absolute ethanol were of analytical grade and purchased from Merck company. The purity and phase composition of the $Bi_{14}W_2O_{27}/Bi_2WO_6$ nanostructures were realized by X-ray diffraction (XRD) analysis on a Bruker AXS D8 Advance, X-ray diffractometer with a Bruker goniometer and Cu-Kα radiation. Fourier transform infrared (FT-IR) spectrum was obtained by a Shimadzu FTIR-8400S spectrometer. The particle size and elemental composition of the $Bi_{14}W_2O_{27}/Bi_2WO_6$ nanocomposites were analyzed by field emission scanning electron microscopy (FE-SEM, Mira3 Tescan) equipped with energy-dispersive X-ray spectroscopy (EDS). UV-Visible diffuse reflectance spectroscopy (UV-Vis DRS) was measured by a Shimadzu UV-2550

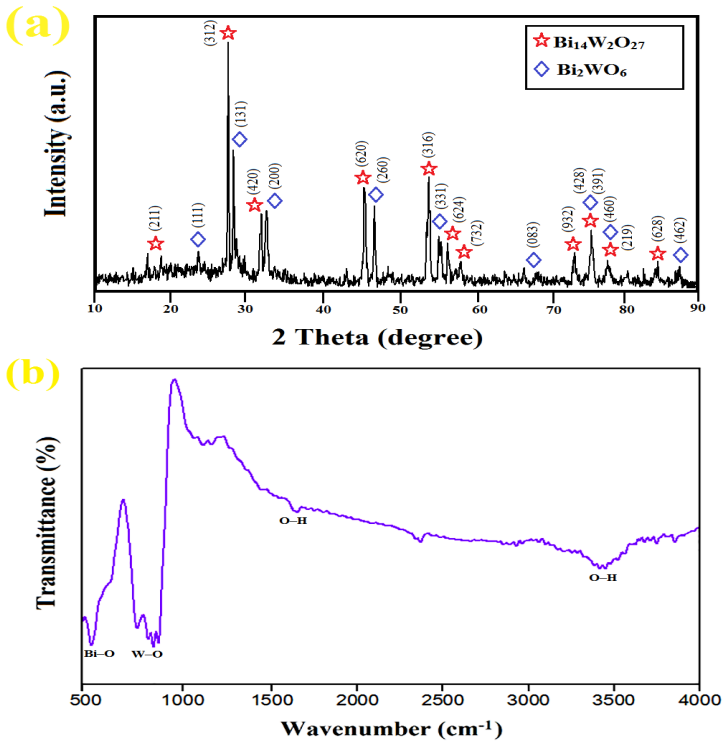

Fig. 1. (a) XRD pattern and (b) FTIR spectra of the $Bi_{14}W_2O_{27}/Bi_2WO_6$ nanostructures (sample 1).

UV-Vis spectrometer. The sulfur values of the photodesulfurized specimens were computed by an X-ray fluorescence sulfur meter (Tanaka Scientific RX-360SH).

Preparation of $Bi_{14}W_2O_{27}/Bi_2WO_6$ nanostructures

The Pechini sol-gel route was employed for the preparation of the $Bi_{14}W_2O_{27}/Bi_2WO_6$ nanocomposites. In this reaction, 16 mmol of $Bi(NO_3)_3.5H_2O$ was dissolved in 10 ml of distilled water containing a little amount of HNO_3. Three mmol of Na_2WO_4 was dissolved in 10 ml of distilled water and added to the above solution under stirring as well. Afterwards, tetracycline was dissolved in 10 ml of distilled water with 0.5:1 mole ratio to total metals and poured into the resulting solution under stirring. Then, PEG-6000 with 1:1 mole ratio to tetracycline was dissolved in 10 ml of distilled water and added to the final mixture. The mixture was heated at 100 °C until the gel-like mixture was allowed to evaporate and then was dried at 80 °C. The as-formed powder calcined at 700 °C for 2 h. In addition, the effect of the chelating agent, gelling agent and mole ratio of chelating agent to total metals on the particle size of the $Bi_{14}W_2O_{27}/Bi_2WO_6$ products were investigated (Table 1).

Photocatalytic desulfurization evaluation

The photocatalytic desulfurization performance of the $Bi_{14}W_2O_{27}/Bi_2WO_6$ nanoparticles was examined by thiophene/hexane solution as model fuel (sulfur concentration was about 500 mg/L). In this process, 50 mg of the $Bi_{14}W_2O_{27}/Bi_2WO_6$ photocatalysts was dispersed in 50 ml of thiophene/hexane fuel and then was aerated with air in dark for 30 min to establish the adsorption/desorption equilibrium. Next, the suspension was irradiated with an Osram 400 W metal halide lamp as simulated sunlight origin. At determined time periods, 5 ml of reaction solution was withdrawn and centrifuged to remove the photocatalyst nanoparticles. The resulting solution and 5 ml of DMF solvent were mixed, and the mixture was stirred for 15 min at room temperature. By this process, the oxidized sulfur compounds in the hexane phase were extracted by the DMF solvent and then the DMF layer was separated by decantation. Finally, the total sulfur in the desulfurized samples was measured by sulfur meter. The desulfurization efficiency (η) of thiophene can be calculated using the following equation:

$$\eta = (S_0 - S_t)/S_0 \times 100 \quad (1)$$

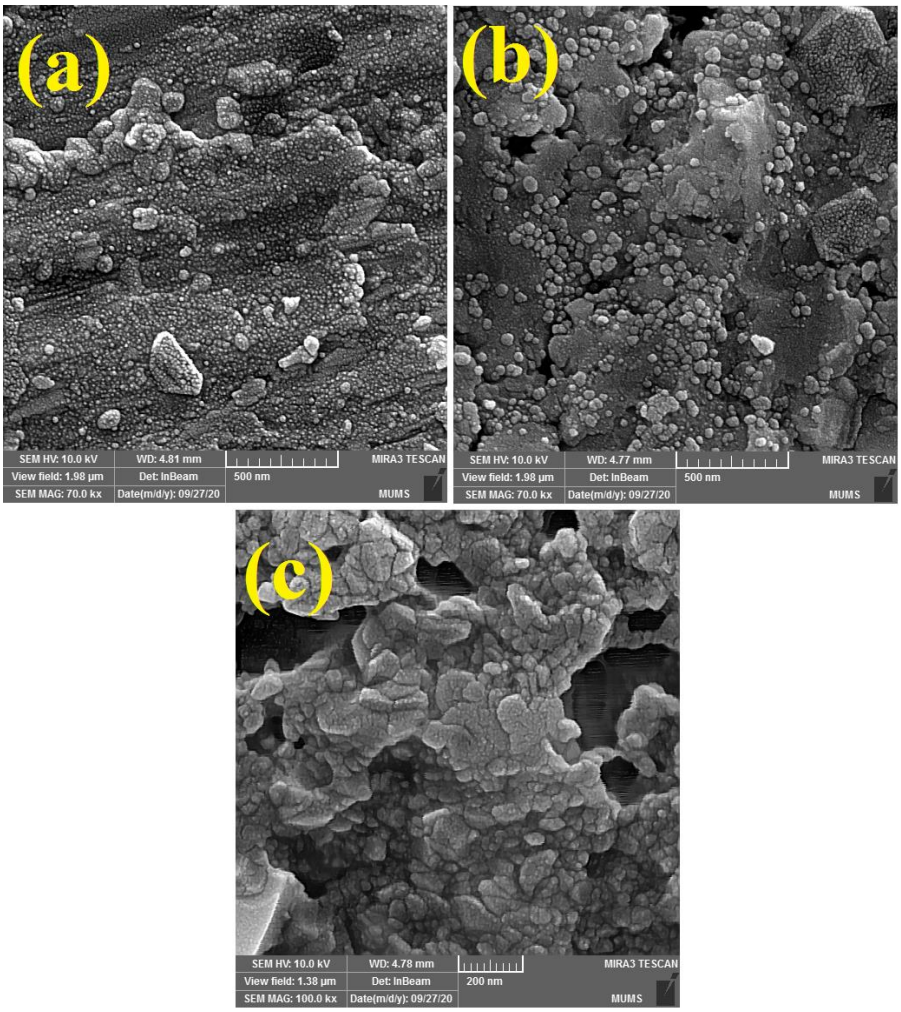

Fig. 2. FESEM images of the $Bi_{14}W_2O_{27}/Bi_2WO_6$ products: (a) sample 1, (b) sample 2 and (c) sample 3.

where S_0 and S_t are the sulfur concentrations in the reaction for initial and t times, respectively.

RESULTS AND DISCUSSION

XRD and FTIR measurements

The crystallographic characteristics and phase composition of the $Bi_{14}W_2O_{27}/Bi_2WO_6$ nanostructures were determined by powder X-ray diffraction (XRD). The XRD pattern of the $Bi_{14}W_2O_{27}/Bi_2WO_6$ product (sample 1) is shown in Fig. 1a. Obviously, the diffraction peaks at 2θ of 17.2°, 27.8°, 32.1°, 45.9°, 54.2°, 56.9°, 58.6°, 73.5°, 76.1°, 78.2° and 84.5° are correspond to the tetragonal phase of the $Bi_{14}W_2O_{27}$ structure (JCPDS Card No. 39-0061). As well as, the characteristic peaks with 2θ of 23.9°, 28.3°, 32.9°, 47.1°, 56.1°, 68.5°, 76.1°, 78.2° and 87.5° that belong to the orthorhombic phase of the Bi_2WO_6 (JCPDS Card No. 39-0256). The XRD pattern indicates the existence of the $Bi_{14}W_2O_{27}$ and Bi_2WO_6 phases in the as-synthesized product. Also, no other impurity peaks of the bismuth tungsten oxides were observed, suggesting high purity of the sample. Finally, the average grain sizes of the $Bi_{14}W_2O_{27}$ and Bi_2WO_6 structures were calculated by the full width at half maxima from their characteristic peaks, which were evaluated to be around 7 and 9 nm, respectively.

Moreover, Fourier transform infrared (FTIR) spectra of the $Bi_{14}W_2O_{27}/Bi_2WO_6$ product (sample 1) was illustrated in Fig. 1b. As can be seen, the transmittance peaks centered at 550 cm^{-1} is assigned to the asymmetry stretching vibrations of Bi–O bands in the sample. In addition, the characteristic peaks located at around 750 to 880 cm^{-1} are attributed to the symmetric and asymmetric stretching vibrations of W–O units

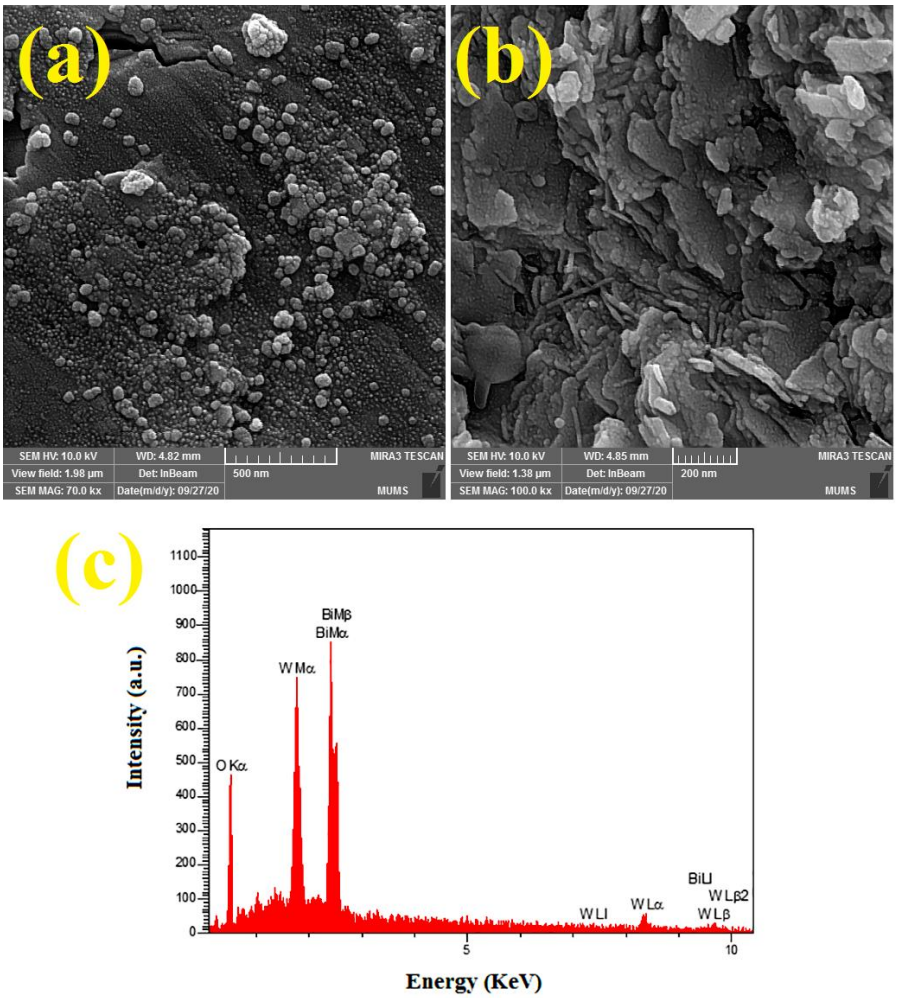

Fig. 3. FESEM images of the $Bi_{14}W_2O_{27}/Bi_2WO_6$ products: (a) sample 4 and (b) sample 5 and (c) EDS spectra of the $Bi_{14}W_2O_{27}/Bi_2WO_6$ (sample 1).

in the $Bi_{14}W_2O_{27}/Bi_2WO_6$. Also, the transmittance peaks situated at 1620 and 3450 cm^{-1} are ascribed to the O–H bending and stretching vibrations of the adsorbed water molecules, respectively [26, 33, 34].

FESEM and EDS measurements

We synthesized the $Bi_{14}W_2O_{27}/Bi_2WO_6$ nanocomposites by Pechini sol-gel method and investigated the influence of the chelating agent, gelling agent and mole ratio of chelating agent to total metals on the particle size of the samples (Table 1). To study the chelating agent type, the $Bi_{14}W_2O_{27}/Bi_2WO_6$ was prepared by various antibiotics such as tetracycline (sample 1), cefixime (sample 2) and sulfanilamide (sample 3) in the presence of PEG-6000 as gelling agent. As depicted in Figs. 2a-c, the ultrafine nanoparticles, sphere-like nanostructures and irregular microstructures were formed by applying tetracycline, cefixime and sulfanilamide, respectively. It seems that in the Pechini sol-gel process, tetracycline as a multidentate chelate, due to its high steric hindrance effect can create a huge polymeric network with PEG-6000, and subsequently control the nucleation and growth of the primary nanoparticles, which leads to the ultrafine morphology of the $Bi_{14}W_2O_{27}/Bi_2WO_6$ nanoparticles [35, 36].

Furthermore, to evaluate the effect of the mole ratio of chelating agent to total metals on the particle size of the $Bi_{14}W_2O_{27}/Bi_2WO_6$ nanostructures, the Pechini synthesis was carried out by 0.5:1 and 1:1 mole ratio of tetracycline to total metals along with PEG-6000 (sample 4). When the mole ratio was about 0.5:1, the ultrafine nanoparticles were formed (Fig. 2a), as well as, by applying 1:1 mole ratio, the regular spherical nanoparticles were achieved (Fig.

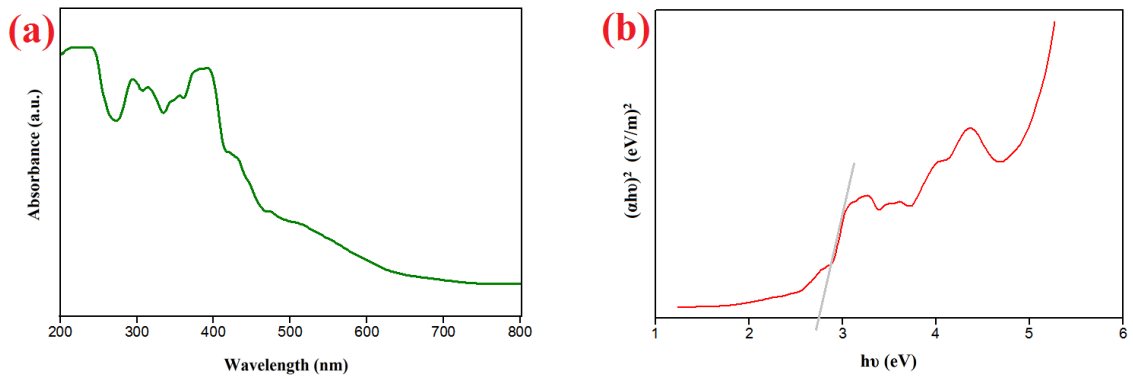

Fig. 4. (a) UV–Vis diffuse reflectance spectra and (b) the plot of $(\alpha h\nu)^2$ against hν to determine the band gap of the $Bi_{14}W_2O_{27}/Bi_2WO_6$ (sample 1).

3a). Moreover, to appraise the effect of the gelling agent on the particle size of the $Bi_{14}W_2O_{27}/Bi_2WO_6$ products, the production process was performed utilizing tepa as gelling agent and tetracycline as chelating agent (sample 5). As demonstrated in Fig. 3b, by using tepa, the sheet-like nanostructures were obtained. Heretofore, PEG-6000 due to its high steric hindrance and effective interactions with tetracycline during the gelation step resulted in the fabrication of ultrafine $Bi_{14}W_2O_{27}/Bi_2WO_6$ nanoparticles (Fig. 2a) [37, 38].

In order to determine the elemental composition of the $Bi_{14}W_2O_{27}/Bi_2WO_6$ product (sample 1), the EDX analysis was carried out. The EDS spectrum of the $Bi_{14}W_2O_{27}/Bi_2WO_6$ sample clearly corroborates the presence of Bi, W, and O elements in the nanocomposite, indicating the high purity of the product (Fig. 3c). Besides, the atomic ratio of Bi:W:O was calculated to be around 16.12:3.18:32.45, respectively, which is close to the stoichiometry value of the $Bi_{14}W_2O_{27}/Bi_2WO_6$.

UV–Vis DRS measurement

UV-Vis DRS was used to investigate the light absorption property of the as-prepared $Bi_{14}W_2O_{27}/Bi_2WO_6$ nanocomposite (sample 1). As illustrated in Fig. 4a, the $Bi_{14}W_2O_{27}/Bi_2WO_6$ nanostructures exhibit enhanced light absorption of both ultraviolet and visible regions with an absorption band edge at around 440 nm. The broad and intense absorption peaks of the $Bi_{14}W_2O_{27}/Bi_2WO_6$ nanocomposite can lead to efficient UV-Vis light harvesting and electron-hole separation in the photocatalyst, and subsequently superior photocatalytic performance under simulated sunlight irradiation. In addition, the band gap energy (Eg) of the $Bi_{14}W_2O_{27}/Bi_2WO_6$ nanostructure can be calculated by the following equation:

$$\alpha h\upsilon = A(h\upsilon - Eg)^2 \quad (2)$$

where α, hυ and A are the absorption coefficient, photonic energy and energy-independent constant, respectively. According to the Tauc plots of $(\alpha h\upsilon)^2$ versus hυ, the Eg value of the sample 1 can be estimated approximately 2.74 eV (Fig. 4b), which provides the $Bi_{14}W_2O_{27}/Bi_2WO_6$ nanocomposite as an efficient photocatalyst for photocatalytic activities under sunlight illumination.

Photocatalytic desulfurization performance and mechanism

The photocatalytic desulfurization performance of the $Bi_{14}W_2O_{27}/Bi_2WO_6$ nanostructures was studied by monitoring the desulfurization of thiophene/hexane solution utilizing air as oxidant and DMF as extraction solvent under simulated sunlight irradiation. As presented in Fig. 5a, the blank experiments suggested that the contribution of the photolysis and the adsorption of thiophene molecules on the photocatalyst surface were insignificant. Therefore, the decomposition of thiophene molecules can only be due to the photocatalytic reactions. The photocatalytic desulfurization efficiency of thiophene over $Bi_{14}W_2O_{27}/Bi_2WO_6$ nanocomposites (sample 1) was obtained ~90% after 120 min of simulated sunlight irradiation (Fig. 5a). A reliable photocatalytic desulfurization mechanism of the $Bi_{14}W_2O_{27}/Bi_2WO_6$ photocatalyst is displayed in Scheme 1. It can be stated that by visible light irradiation in the photocatalytic system, the $Bi_{14}W_2O_{27}/Bi_2WO_6$ nanoparticle can absorb the incident photons and simultaneously generate the electrons and holes on its conductive band (CB) and valance band

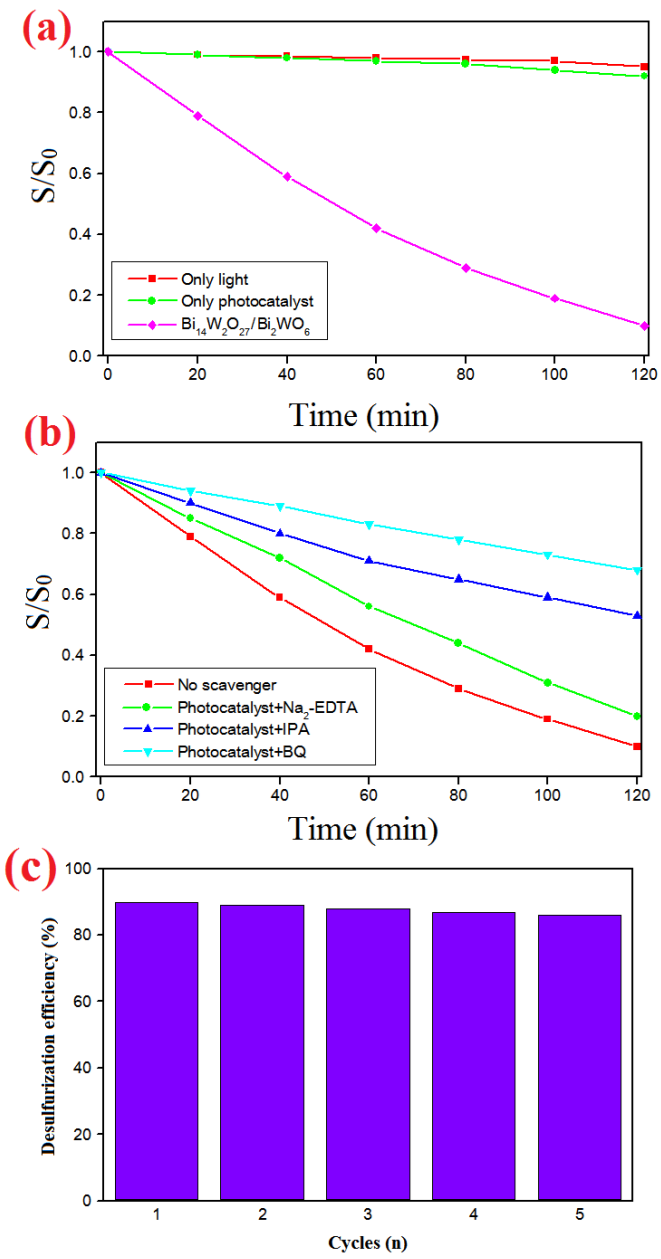

Fig. 5. (a) Photodesulfurization curves of thiophene over $Bi_{14}W_2O_{27}/Bi_2WO_6$ (sample 1), (b) radical trapping experiment and (c) the photocatalytic stability of the $Bi_{14}W_2O_{27}/Bi_2WO_6$ (sample 1).

(VB), respectively. Subsequently, the accumulated electrons in the CB can interact with the adsorbed O_2 molecules and generate superoxide anion radicals ($^{\bullet}O_2^-$). Meanwhile, the stored holes in the VB can oxidize the H_2O or OH^- species to produce hydroxyl radicals ($^{\bullet}OH$). These oxidative $^{\bullet}O_2^-$ and $^{\bullet}OH$ species can attack to the sulfur atoms in thiophene and oxidize them to yield thiophene-S-oxide compounds. The excellent photocatalytic desulfurization activity of the $Bi_{14}W_2O_{27}/Bi_2WO_6$ photocatalyst can be attributed to the powerful visible-light absorption, ultrafine nanoparticle, and high separation and low recombination of charge carriers [39-41].

Furthermore, we compared the photocatalytic desulfurization activity of the present $Bi_{14}W_2O_{27}/Bi_2WO_6$ nanocomposite (sample 1) with other compounds. As can be seen in Table 2, the

Table 2. Comparison of photocatalytic desulfurization performance of our-synthesized $Bi_{14}W_2O_{27}/Bi_2WO_6$ nanocomposite with other materials reported in previous works.

Photocatalyst	Sulfur source	Irradiation time (min)	Desulfurization efficiency (%)	Ref.
$Cu/Cu_2O/BiVO_4/Bi_7VO_{13}$	Thiophene	150	92	[42]
Cu_2O-CeO_2	Thiophene	180	84	[43]
AgI/Bi_2O_3	Dibenzothiophene	120	93	[44]
$AgBiS_2$	Thiophene	120	89	[45]
$Bi_{14}W_2O_{27}/Bi_2WO_6$	Thiophene	120	90	[This work]

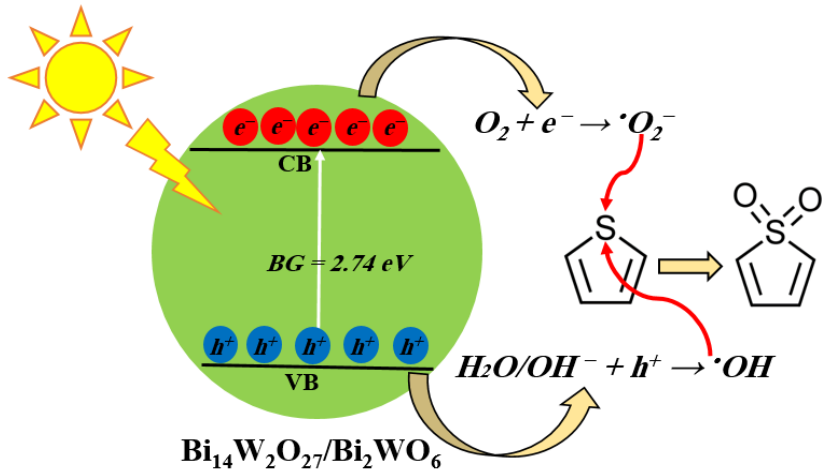

Scheme 1. Schematic mechanism for photocatalytic desulfurization performance of the $Bi_{14}W_2O_{27}/Bi_2WO_6$ product (sample 1).

$Bi_{14}W_2O_{27}/Bi_2WO_6$ photocatalyst shows higher desulfurization efficiency of thiophene than other materials after 120 min of simulated sunlight irradiation. This result suggests that the $Bi_{14}W_2O_{27}/Bi_2WO_6$ nanocomposite photocatalyst can be applied as an efficient material for photocatalytic desulfurization applications.

It is well known that the photoinduced reactive radicals by photocatalytic reactions characterize the photocatalytic pathway of a photocatalyst. Hence, the radical trapping in the $Bi_{14}W_2O_{27}/Bi_2WO_6$ nanostructures (sample 1) was investigated by employing BQ, IPA and Na_2-EDTA as scavenger of superoxide (${}^{\bullet}O_2^-$), hydroxyl (${}^{\bullet}OH$) and hole (h^+), respectively, under the same conditions. As illustrated in Fig. 5b, BQ, IPA and Na_2-EDTA can reduce the desulfurization efficiency from 90% to 32%, 47% and 80%, respectively. This result proposes that the ${}^{\bullet}O_2^-$ and ${}^{\bullet}OH$ radicals are the major species in the photocatalytic desulfurization of thiophene by $Bi_{14}W_2O_{27}/Bi_2WO_6$ nanocomposite.

Furthermore, we evaluated the recyclability of the $Bi_{14}W_2O_{27}/Bi_2WO_6$ nanoparticles (sample 1) for photodesulfurization of thiophene under simulated sunlight irradiation. The photocatalytic desulfurization performance of the as-synthesized photocatalyst slightly decreased after five sequential runs (Fig. 5c), indicating high stability of the $Bi_{14}W_2O_{27}/Bi_2WO_6$ photocatalyst for photocatalytic applications.

CONCLUSIONS

In summary, we synthesized $Bi_{14}W_2O_{27}/Bi_2WO_6$ photocatalyst via a Pechini sol-gel method utilizing tetracycline as chelating agent and PEG-6000 as gelling agent. Also, the effect of the chelating agent,

gelling agent and mole ratio of chelating agent on total metals was investigated. The ultrafine $Bi_{14}W_2O_{27}/Bi_2WO_6$ nanoparticles were applied for photocatalytic desulfurization of thiophene, which showed that the as-fabricated product had superior photocatalytic desulfurization of thiophene (~90%) after 120 min of simulated sunlight irradiation. Moreover, the band gap energy of the $Bi_{14}W_2O_{27}/Bi_2WO_6$ nanocomposite was about 2.74 eV. The promoted photodesulfurization of the $Bi_{14}W_2O_{27}/Bi_2WO_6$ nanostructures can be related to the enhanced photon absorption, ultrafine morphology, and high separation and low recombination of charge couples. Based on the radical trapping experiment, a photocatalytic desulfurization workmanship was expressed, which represented that the $^{\bullet}O_2^-$ and $^{\bullet}OH$ radicals have a notable contribution in the photocatalytic desulfurization process. The solar-driven, high activity, notable recyclability, and simple production of the $Bi_{14}W_2O_{27}/Bi_2WO_6$ nanocomposite are promising for the photocatalytic fields in various industries.

ACKNOWLEDGMENTS

Authors are thankful to the council of Iran National Science Foundation and Islamic Azad University branch of Birjand for supporting this work.

CONFLICT OF INTEREST

The authors declare no conflict of interest.

REFERENCES

1 O. Amiri, F. Beshkar, S.S. Ahmed, P.H. Mahmood, A.A. Dezaye, Hierarchical p-BiOI/n-BiPO4 heterojunction nanocomposite with enhanced visible-light photocatalytic desulfurization of thiophene under mild conditions, Int. J. Hydrog. Energy. 46 (2021) 6547-6560. https://doi.org/10.1016/j.ijhydene.2020.11.181

2 O. Amiri, F. Beshkar, S.S. Ahmed, A. Rafiei-Miandashti, P.H. Mahmood, A.A. Dezaye, Novel flower-like (Bi(Bi2S3)9I3)2/3 nanostructure as efficient photocatalyst for photocatalytic desulfurization of benzothiophene under visible light irradiation, Adv. Powder Technol. 32 (2021) 1088-1098. https://doi.org/10.1016/j.apt.2021.02.012

3 O. Amiri, F. Beshkar, S.S. Ahmed, B.W. Hamad, P.H. Mahmood, A.A. Dezaye, Magnetically-driven Ag/Fe3O4/graphene ternary nanocomposite as efficient photocatalyst for desulfurization of thiophene under visible-light irradiation, Int. J. Hydrog. Energy. (2021) https://doi.org/10.1016/j.ijhydene.2021.03.072. https://doi.org/10.1016/j.ijhydene.2021.03.072

4 W.S.A. Rahma, F.S. Mjalli, T. Al-Wahaibi, A.A. Al-Hashmi, Polymeric-based deep eutectic solvents for effective extractive desulfurization of liquid fuel at ambient conditions, Chem. Eng. Res. Des. 120 (2017) 271-283. https://doi.org/10.1016/j.cherd.2017.02.025

5 G. Chen, W. Xie, Q. Li, W. Wang, L. Bing, F. Wang, G. Wang, C. Fan, S. Liu, D. Han, Three-dimensionally ordered macro-mesoporous CoMo bulk catalysts with superior performance in hydrodesulfurization of thiophene, RSC Adv., 10 (2020) 37280-37286. https://doi.org/10.1039/D0RA07153F

6 J.B. Bhasarkar, S. Chakma, V.S. Moholkar, Investigations in physical mechanism of the oxidative desulfurization process assisted simultaneously by phase transfer agent and ultrasound. Ultrason. Sonochem. 24 (2015) 98–106. https://doi.org/10.1016/j.ultsonch.2014.11.008

7 X. Lu, X. Li, F. Chen, Z. Chen, J. Qian, Q. Zhang, Biotemplating synthesis of N-doped two-dimensional CeO2-TiO2 nanosheets with enhanced visible light photocatalytic desulfurization performance, J. Alloys Compd. 815 (2020) 152326. https://doi.org/10.1016/j.jallcom.2019.152326

8 M. Mousavi-Kamazani, Cube-like Cu/Cu2O/BiVO4/Bi7VO13 composite nanoparticles: Facile sol-gel synthesis for photocatalytic desulfurization of thiophene under visible light, J. Alloys Compd. 823 (2020) 153786. https://doi.org/10.1016/j.jallcom.2020.153786

9 M. Mousavi-Kamazani, M. Shirani, F. Beshkar, S. Mortazavi-Derazkola, One-step ultrasonic production of novel worm-like Bi7(PO4)O9 photocatalyst for efficient degradation of ciprofloxacin antibiotic under simulated solar light, J. Mater. Sci. Mater. Electron. 31 (2020) 19657-19671. https://doi.org/10.1007/s10854-020-04492-3

10 D. Ghanbari, M. Salavati-Niasari, S. Khaghani, F. Beshkar, Preparation of polyvinyl acetate (PVAc) and PVAc-Ag-Fe3O4 composite nanofibers by electro-spinning method, J. Clust. Sci. 27 (2016) 1317-1333. https://doi.org/10.1007/s10876-016-1002-2

11 M. Mousavi-Kamazani, R. Rahmatolahzadeh, S.A. Shobeiri, F. Beshkar, Sonochemical synthesis, formation mechanism, and solar cell application of tellurium nanoparticles, Ultrason. Sonochem. 39 (2017) 233-239. https://doi.org/10.1016/j.ultsonch.2017.04.031

12 F. Beshkar, O. Amiri, M. Salavati-Niasari, F. Beshkar, Novel dendrite-like CuCr2O4 photocatalyst prepared by a simple route in order to remove of Azo Dye in textile and dyeing wastewater, J. Mater. Sci. Mater. Electron. 26 (2015) 8182-8192. https://doi.org/10.1007/s10854-015-3479-0

13 J. Wu, J. Li, J. Liu, J. Bai, L. Yang, A novel Nb2O5/Bi2WO6 heterojunction photocatalytic oxidative desulfurization catalyst with high visible light-induced photocatalytic activity, RSC Adv., 7 (2017) 51046-51054. https://doi.org/10.1039/C7RA09829D

14 J. Cui, G. Wang, W. Liu, P. Ke, Q. Tian, X. Li, Y. Tian, Synthesis Synthesis BiVO4 modified by CuO supported onto bentonite for molecular oxygen photocatalytic oxidative desulfurization of fuel under visible light, Fuel 290 (2021) 120066. https://doi.org/10.1016/j.fuel.2020.120066

15 S. Lei, C. Yang, H. Liao, J. Chen, J. Zhong, J. Li, Enhanced photocatalytic activity of N134 carbon black modified Bi2WO6 benefited from ample oxygen vacancies and boosted separation of photoexcited carriers, Mater. Res. Bull. 133 (2021) 111075. https://doi.org/10.1016/j.materresbull.2020.111075

16 M. Kodols, S. Didrihsone, J. Grabis, Bi2WO6 nanoparticles

prepared by combustion synthesis with different fuels and their photocatalytic activity, Key Eng. Mater. 604 (2014) 93-101. https://doi.org/10.4028/www.scientific.net/KEM.604.93

17 J. Sun, C.H. Shen, J. Guo, H. Guo, Y.F. Yin, X.J. Xu, Z.H. Fei, Z.T. Liu, X.J. Wen, Highly efficient activation of peroxymonosulfate by Co3O4/Bi2WO6 p-n heterojunction composites for the degradation of ciprofloxacin under visible light irradiation, J. Colloid Interface Sci. 588 (2021) 19-30. https://doi.org/10.1016/j.jcis.2020.12.043

18 J. Tian, Z. Zhu, B. Liu, Novel Bi2MoO6/Bi2WO6/MWCNTs photocatalyst with enhanced photocatalytic activity towards degradation of RB-19 under visible light irradiation, Colloids Surf. A 581 (2019) 123798. https://doi.org/10.1016/j.colsurfa.2019.123798

19 F. Opoku, K.K. Govender, C.G.C.E. van Sittert, P.P. Govender, Insights into the photocatalytic mechanism of mediator-free direct Z-scheme g-C3N4/Bi2MoO6(010) and g-C3N4/Bi2WO6(010) heterostructures: A hybrid density functional theory study, Appl. Surf. Sci. 427 (2018) 487-498. https://doi.org/10.1016/j.apsusc.2017.09.019

20 A. Yuan, H. Lei, Z. Wang, X. Dong, Improved photocatalytic performance for selective oxidation of amines to imines on graphitic carbon nitride/bismuth tungstate heterojunctions, J. Colloid Interface Sci. 560 (2020) 40-49. https://doi.org/10.1016/j.jcis.2019.10.060

21 I. Das, Md.T. Noori, G.D. Bhowmick, M.M. Ghangrekar, Synthesis of tungstate oxide/bismuth tungstate composite and application in microbial fuel cell as superior low-cost cathode catalyst than platinum, J. Electrochem. Soc. 165 (2018) G146. https://doi.org/10.1149/2.0781813jes

22 P.F. Cao, S.Y. Ma, X.L. Xu, Novel ultra-sensitive dandelion-like Bi2WO6 nanostructures for ethylene glycol sensing application, Vacuum 181 (2020) 109748. https://doi.org/10.1016/j.vacuum.2020.109748

23 Q. Wang, H. Li, X. Yu, Y. Jia, Y. Chang, S. Gao, Morphology regulated Bi2WO6 nanoparticles on TiO2 nanotubes by solvothermal Sb3+ doping as effective photocatalysts for wastewater treatment, Electrochim. Acta. 330 (2020) 135167. https://doi.org/10.1016/j.electacta.2019.135167

24 J. Hu, D. Chen, Z. Mo, N. Li, Q. Xu, H. Li, J. He, H. Xu, J. Lu, Z-scheme 2D/2D heterojunction of black phosphorus/monolayer Bi2WO6 nanosheets with enhanced photocatalytic activities, Angew. Chem. Int. Ed. 58 (2019) 2073-2077. https://doi.org/10.1002/anie.201813417

25 J. Huang, X. Li, G. Su, R. Gao, W. Wang, B. Dong, L. Cao, Construction of layer-by-layer g-C3N4/Ag/Bi2WO6 Z-scheme system with enhanced photocatalytic activity, J. Mater. Sci. 53 (2018) 16010-16021. https://doi.org/10.1007/s10853-018-2672-y

26 M. Ranjeh, F. Beshkar, O. Amiri, M. Salavati-Niasari, H. Moayedi, Pechini sol-gel synthesis of Cu2O/Li3BO3 and CuO/Li3BO3 nanocomposites for visible light-driven photocatalytic degradation of dye pollutant, J. Alloy Compd. 815 (2020) 152451. https://doi.org/10.1016/j.jallcom.2019.152451

27 M. Saghi, A. Shokri, A. Arastehnodeh, M. Khazaeinejad, A. Nozari, The photo degradation of methyl red in aqueous solutions by α-Fe2O3/SiO2 nano photocatalyst, J. Nanoanalysis., 5 (2018) 163-170.

28 R. Hekmatshoar, A.R. Yari, A. Shokri, Using ZnO based on Bentonite as a nano photocatalyst for degradation of Acid Red 114 in synthetic wastewater, J. Nanoanalysis., 7 (2020) -10.

29 A. Shokri, An investigation of carbon nanotubes on shear stress, thermal conductivity and the viscosity of Nanofluids, J. Nanoanalysis., 7 (2020) -7.

30 A. Shokri, S. Karimi, The removal of Hexavalent chromium; (Cr (VI)) by ZnO/LECA as a nano photocatalyst using full factorial experimental design, J. Nanoanalysis., (2021), Doi: 10.22034/JNA.2021.1906290.1223.

31 F. Beshkar, M. Salavati-Niasari, O. Amiri, Facile one-pot in situ synthesis and characterization of a Cu2O/Cu2(PO4)(OH) binary heterojunction nanocomposite for the efficient photocatalytic degradation of ciprofloxacin from aqueous solution under direct sunlight irradiation, Ind. Eng. Chem. Res. 60 (2021) 9578-9591. https://doi.org/10.1021/acs.iecr.1c01462

32 M. Mousavi-Kamazani, Facile sonochemical-assisted synthesis of Cu/ZnO/Al2O3 nanocomposites under vacuum: Optical and photocatalytic studies, Ultrasonics Sonochemistry, 58 (2019) 104636. https://doi.org/10.1016/j.ultsonch.2019.104636

33 Y. Geng, P. Zhang, S. Kuang, Fabrication and enhanced visible-light photocatalytic activities of BiVO4/Bi2WO6 composites, RSC Adv., 4 (2014) 46054-46059. https://doi.org/10.1039/C4RA07427K

34 Ji. Huang, X. Li, G. Su, R. Gao, W. Wang, B. Dong, L. Cao, Construction of layer-by-layer g-C3N4/Ag/Bi2WO6 Z-scheme system with enhanced photocatalytic activity, J. Mater. Sci. 53 (2018) 16010-16021. https://doi.org/10.1007/s10853-018-2672-y

35 M. Valian, F. Beshkar, M. Salavati-Niasari, Two facile methods to produce the cobalt manganite nanostructures and evaluation of their photocatalytic performance, J. Mater. Sci. Mater. Electron. 28 (2017) 6292-6300. https://doi.org/10.1007/s10854-016-6312-5

36 F. Namvar, F. Beshkar, M. Salavati-Niasari, S. Bagheri, Morphology-controlled synthesis, characterization and photocatalytic property of hierarchical flower-like Dy2Mo3O9 nanostructures, J. Mater. Sci. Mater. Electron. 28 (2017) 10313-10320. https://doi.org/10.1007/s10854-017-6799-4

37 M. Valian, F. Beshkar, M. Salavati-Niasari, Urchin-like Dy2CoMnO6 double perovskite nanostructures: new simple fabrication and investigation of their photocatalytic properties, J. Mater. Sci. Mater. Electron. 28 (2017) 12440-12447. https://doi.org/10.1007/s10854-017-7065-5

38 D. Ghanbari, M. Salavati-Niasari, F. Beshkar, O. Amiri, Electro-spinning of cellulose acetate nanofibers: microwave synthesize of calcium ferrite nanoparticles and CA-Ag-CaFe2O4 nanocomposites, J. Mater. Sci. Mater. Electron. 26 (2015) 8358-8366. https://doi.org/10.1007/s10854-015-3502-5

39 M. Ranjeh, F. Beshkar, M. Salavati-Niasari, Sol-gel synthesis of novel Li-based boron oxides nanocomposite for photodegradation of azo-dye pollutant under UV light irradiation, Compos Part B: Eng, 172 (2019) 33-40. https://doi.org/10.1016/j.compositesb.2019.05.085

40 H.A. Alshamsi, F. Beshkar, O. Amiri, M. Salavati-Niasari, Porous hollow Ag/Ag2S/Ag3PO4 nanocomposites as highly efficient heterojunction photocatalysts for the removal of antibiotics under simulated sunlight irradiation, Chemosphere, 274 (2021) 129765. https://doi.org/10.1016/j.chemosphere.2021.129765

41 S.A. Shobeiri, M. Mousavi-Kamazani, F. Beshkar, Facile mechanical milling synthesis of NiCr2O4 using novel organometallic precursors and investigation of its photocatalytic activity, J. Mater. Sci. Mater. Electron. 28 (2017) 8108-8115. https://doi.org/10.1007/s10854-017-6517-2

42 M. Mousavi-Kamazani, Cube-like Cu/Cu2O/BiVO4/Bi7VO13 composite nanoparticles: Facile sol-gel synthesis for photocatalytic desulfurization of thiophene under visible light, J. Alloys Compd. 823 (2020) 153786. https://doi.org/10.1016/j.jallcom.2020.153786

43 M. Mousavi-Kamazani, S. Ashrafi, Single-step sonochemical synthesis of Cu2O-CeO2 nanocomposites with enhanced photocatalytic oxidative desulfurization, Ultrason. Sonochem. 63 (2020) 104948. https://doi.org/10.1016/j.ultsonch.2019.104948

44 M. Mousavi-Kamazani, M. Ghodrati, R. Rahmatolahzadeh, Fabrication of Z-scheme flower-like AgI/Bi2O3 heterojunctions with enhanced visible light photocatalytic desulfurization under mild conditions, J. Mater. Sci. Mater. Electron. 31 (2020) 5622-5634. https://doi.org/10.1007/s10854-020-03129-9

45 M. Mousavi-Kamazani, R. Rahmatolahzadeh, H. Najafian, Efficient photocatalytic desulfurization of thiophene under visible light irradiation over flower-like AgBiS2 photocatalyst, J. Nanoanalysis., 7 (2020) 248-261.